HHS Public Access

Author manuscript

Clin Cancer Res. Author manuscript; available in PMC 2024 July 17.

Published in final edited form as:

Clin Cancer Res. 2024 January 17; 30(2): 420–435. doi:10.1158/1078-0432.CCR-23-0433.

CDK4/6 inhibition sensitizes intracranial tumors to PD-1 blockade in preclinical models of brain metastasis

Naema Nayyar[1,2], **Magali A de Sauvage**[2], **Jane Chuprin**[1], **Emily M Sullivan**[2], **Mohini Singh**[2], **Consuelo Torrini**[2], **Britney S Zhang**[2], **Sushobhana Bandyopadhyay**[1,3], **Keith A Daniels**[1], **Christopher Alvarez-Breckenridge**[2,4], **Ashish Dahal**[2], **Michael A Brehm**[2,*], **Priscilla K Brastianos**[2,5,†,*]

[1]Program in Molecular Medicine, UMass Chan Medical School, Worcester, MA

[2]Center for Cancer Research, Massachusetts General Hospital, Boston, MA

[3]Gene Therapy Program, Perelman School of Medicine, University of Pennsylvania

[4]Department of Neurosurgery, The University of Texas MD Anderson Cancer Center, Houston, TX

[5]Department of Medicine, Harvard Medical School and Massachusetts General Hospital, Boston, Massachusetts

Abstract

Purpose: Brain metastases are associated with high morbidity and often resistant to immune checkpoint inhibitors. We evaluated whether CDK4/6 inhibitor (CDKi) abemaciclib can sensitize intracranial tumors to PD-1 inhibition in mouse models of melanoma and breast cancer brain metastasis.

Experimental Design: Treatment response was evaluated in vivo using immunocompetent mouse models of brain metastasis bearing concurrent intracranial and extracranial tumors. Treatment effect on intracranial and extracranial tumor immune microenvironments was evaluated using immunofluorescence, multiplex immunoassays, high-parameter flow cytometry and T cell receptor profiling. Mice with humanized immune systems were evaluated using flow cytometry to study the effect of CDKi on human T cell development.

Results: We found that combining abemaciclib with PD-1 inhibition reduced tumor burden and improved overall survival in mice. The tumor immune microenvironment, which differed based on anatomical location of tumors, was altered with CDKi and PD-1 inhibition in an organ-specific manner. Combination abemaciclib and anti-PD-1 treatment increased recruitment and expansion of $CD8^+$ effector T cell subsets, depleted $CD4^+$ regulatory T (T_{REG}) cells, and reduced levels of immunosuppressive cytokines in intracranial tumors. In immunodeficient mice engrafted with human immune systems, abemaciclib treatment supported development and maintenance of $CD8^+$ T cells and depleted T_{REG} cells.

[†]**Corresponding author:** Priscilla Brastianos, MD, 55 Fruit Street, Yawkey 9E, Boston, MA 02114, USA. pbrastianos@mgh.harvard.edu; Phone: 617-724-0641.

[*]These authors jointly supervised this work

Conclusions: Our results highlight the distinct properties of intracranial and extracranial tumors and support clinical investigation of combination CDK4/6 and PD-1 inhibition in patients with brain metastases.

INTRODUCTION

Therapies targeting immune regulatory receptors such as programmed death receptor 1 (PD-1) and cytotoxic T lymphocyte associate antigen 4 (CTLA-4) have transformed the management of advanced cancers, generating long-term regression of tumors in some patients (1). Response to immune checkpoint inhibitors (ICIs) in patients with central nervous system (CNS) metastases is an active area of investigation. In patients with parenchymal brain metastases, durable intracranial treatment responses are limited and a subset of patients experience intracranial progression despite systemic disease control (2–5). Studies of dual-agent ICI therapy combining PD-1 and CTLA-4 antagonists demonstrate increased intracranial efficacy relative to single-agent ICI administration (2). However, dual-agent ICI is associated with high toxicity; 55% of patients experience serious (grade 3 or higher) immune-related adverse events (irAEs) (2,6). The poor prognosis associated with brain metastases, particularly amongst symptomatic lesions, and morbidity of current treatment options necessitate development of more effective and less toxic combinatorial therapeutic approaches that can sensitize intracranial tumors to immunotherapies and extend survival.

Cyclin-dependent kinases 4 and 6 (CDK4/6) bind to D-type cyclins to integrate mitogenic signals and drive cell cycle progression through G1 phase. Genomic alterations that result in deregulation of CDK4/6 drive initiation and progression of cancers. CDK4/6 pathway alterations are therefore prevalent in most cancers, occurring in up to 90% of melanomas (7,8), and especially common in brain metastases (9,10). Studies have also linked aberrant CDK4/6 function with immune evasion, orchestrating an immunologically cold tumor microenvironment and conferring resistance to immunotherapy (11–13). Selective, small-molecule CDK4/6 inhibitors (CDKi) such as abemaciclib, palbociclib and ribociclib have shown promising results in the clinic, receiving FDA approval as first line therapy for hormone receptor positive, HER2-negative breast cancers (14). Importantly, these inhibitors have also demonstrated intracranial benefit in patients with brain metastases (15,16). Abemaciclib specifically is known to be CNS penetrant, exhibiting improved delivery into intracranial tumors compared to palbociclib in pre-clinical studies and exceeding therapeutic concentrations in human brain metastases (16,17). However, investigation of rational drug combination strategies is imperative to circumvent acquired resistance and enhance disease control in patients.

In addition to tumor growth inhibition via cell cycle arrest, CDKi can enhance anti-tumor immunity and induce tumor regression in preclinical as well as clinical studies (18,19). CDKi-mediated inflammation of the tumor microenvironment increases antigen presentation on tumor cells and T cell infiltration into tumors (19–21). CDKi also acts on immune cells directly, enhancing activation of antigen-experienced T cells and reducing proliferation of immunosuppressive T_{REG} cells (19,20). Importantly, CDK4 activity is inversely correlated with PD-L1 levels, and CDKi reportedly stabilizes PD-L1 expression on tumor cells,

providing a strong rationale for combining CDKi with PD-1/PD-L1 antagonists. Several studies have demonstrated the therapeutic efficacy of combined CDK and PD-1/PD-L1 inhibition in extracranial tumor models (11,19–22).

Whether the anti-tumor immunity elicited by CDKi extends to brain metastases remains unexplored. In this study, we evaluated the efficacy of combining CDKi (abemaciclib) and anti-PD-1 therapy ("combination therapy") in mouse models of brain metastases, elucidated how combination therapy remodeled the tumor immune microenvironment (TIME) and T cell receptor (TCR) repertoires, and investigated the effects of CDKi on T cell development and maintenance in NOD-*scid Il2rg*^{null} (NSG) mice engrafted with human immune systems ("humanized mice"). Our findings offer a strong rationale for the clinical evaluation of combination CDKi and PD-1 blockade in patients with brain metastases.

MATERIALS AND METHODS

Cell culture.

YUMM1.7, B16-F10 and 4T1 cells were obtained from American Type Culture Collection (Cat#/RRID: CRL-3362/CVCL_JK16, CRL-6475/CVCL_0159, CRL-2539/ CVCL_0125). YUMM1.7 cells were cultured in DMEM/F12 media (Cat# 11-320-033, Gibco) with 1X non-essential amino acids (Cat# 13–114E, Lonza), B16-F10 cells were cultured in DMEM media (Cat# 10-013-CV, Gibco) and 4T1 cells were cultured in RPMI1640 media (RPMI, Cat# 11875093, Gibco). All media were supplemented with 10% fetal bovine serum (Cat# A3160402, Gibco) and 1X antibiotic/antimycotic (Cat# 15240062, Gibco) and cultured at 37°C with 5% CO_2. Cells were transduced with Firefly luciferase and mCherry expression construct as previously described (10). Cell lines were tested for mycoplasma every few months (most recently in October 2022) and passaged 2–4 times prior to use in experiments.

Animal Studies.

All *in vivo* experiments were approved by the Institutional Animal Care and Use Committee at Massachusetts General Hospital or University of Massachusetts (UMass) Chan Medical School. Experiments in immunocompetent mice involved 6–8 week old female C57BL/6 and BALB/c mice sourced from Charles River Laboratories and housed in a 12-hour light-dark cycle with free access to food and water. 5-week-old female NOD.*Cg-Prkdc*^{scid}*Il2rg*^{tm1Wjl}/SzJ (NOD-*scid IL2r*γ^{null}, NSG) mice were acquired from The Jackson Laboratory and housed in a specific pathogen-free facility in microisolator cages with free access to autoclaved food and acidified autoclaved water.

Subcutaneous tumor implantation.

Right flanks of mice were shaved and cleaned using alcohol prep pads. Tumor cells were resuspended in HBSS (2×10^5 cells/50 uL) and injected subcutaneously using sterile 0.5 mL 28-gauge insulin syringes. Tumors were measured in two dimensions using electronic calipers and tumor volumes were calculated as (length x width^2)/2. Mice were monitored daily for general health and ulceration of tumors and sacrificed if tumors reached 20 mm in diameter or lost more than 30% of their body weight.

Mammary fat pad tumor implantation.

Tumor cells were resuspended in HBSS (2×10^5 cells/50 uL) and injected into the inguinal (fourth) mammary glands using sterile 0.5 mL 28-gauge insulin syringes. Mice were monitored daily for general health and ulceration of tumors and sacrificed if tumors reached 20 mm in diameter or lost more than 30% of their body weight.

Intracranial tumor implantation.

3 days after subcutaneous or mammary fat pad injection, mice were anesthetized with 40–50 mg/kg of sodium pentobarbital (Nembutol) and placed in a stereotaxic frame (David Kopf Instruments). Following disinfection of the incision site with betadine and 70% ethanol, tumor cells suspended in 2 μL HBSS were injected into the right mid-striatum (2.5 mm lateral from bregma and 2.5 mm deep) using a 26-gauge syringe (Hamilton Company). 1×10^4 YUMM1.7 cells were used for abemaciclib and CD8-depletion experiment, 5×10^4 YUMM1.7 cells were used for experiments where tumor tissue was harvested for analysis, 1×10^4 YUMM1.7-FmC cells, 5×10^3 B16-F10 cells and 2×10^4 4T1-FmC cells were used for combination therapy efficacy experiments. MediGel CPF cups (Cat# 74-05-5022, ClearH2O) or Rimadyl tablets (Cat# MD150–2, Bio-Serv) were administered for pain management. Mice were monitored daily for general health and euthanized when severe neurological symptoms developed or when they lost more than 30% of their body weight. In animals with dual extracranial/intracranial tumors where no luciferase tag was used to monitor intracranial tumor burden, overall survival calculations were based on animals euthanized upon development of neurological symptoms.

Human HSC isolation and engraftment into NSG mice.

Human umbilical cord blood was provided by UMass Memorial Umbilical Cord Blood Donation Program, in accordance with the Committee for the Protection of Human Subjects in Research guidelines provided by UMass Chan Medical School. 5-week-old NSG mice were irradiated with 100 cGy and 5×10^4 CD34+ HSCs derived from umbilical cord blood from a single donor were injected via tail vein (23). Peripheral blood was collected from submandibular (facial) veins of mice 15 weeks later and 19 weeks later and analyzed by flow cytometry to confirm engraftment and development of the human immune system. Mice with >10% hCD45+ cells and >2% human CD3+ T cells were considered successfully engrafted and enrolled in study (Table S1).

In vivo administration of therapy and depletion antibodies.

Abemaciclib was dissolved in 1% HEC in 25 mM phosphate buffer at pH 2–2.2 at 20 mg/mL and stored at −20°C or at 4°C for up to 7 days. Immunocompetent mice were dosed with 90 mg/kg abemaciclib and NSG mice were dosed with 75 mg/kg abemaciclib daily by oral gavage for up to 14 days. Antibodies against PD-1 (Cat# BE0146; RRID: AB_10949053), CTLA-4 (Cat# BE0131; RRID: AB_10950184) and CD8a (Cat# BE0061) or isotype control antibodies (Cat# BE0089, BE0087, BE0090, respectively) were obtained from BioXCell and diluted to 2 μg/mL in *InVivo*Pure pH 7.0 dilution buffer (Cat# IP0070). Antibodies were dosed at 10 mg/kg by intraperitoneal injection every 3 days, except anti-CD8a antibody which was administered every 4 days.

Bioluminescence imaging.

Mice were anesthetized with 3% isoflurane in 100% oxygen, injected with 4.5 mg/kg of D-luciferin in 300 μL saline, and imaged after 10 minutes using an optical imaging platform (Spectral Instruments Imaging). Images were taken every 5 minutes until photon counts peaked. Tumor burden was estimated by measuring the photon intensity above the background signal in a region of interest and normalized by area.

Immunofluorescence staining and microscopy.

Formalin fixed paraffin embedded tumor samples were sectioned at 5 μm thickness onto glass slides, then deparaffinized in xylene for two 10-minute washes. They were then rehydrated in 100%, 90%, and 70% ethanol for five minutes each, followed by a rinse step in phosphate buffered saline. The slides were boiled in 1X Citrate Buffer pH 6.0 (Cat# 60493, Abcam) 20 minutes, cooled, and washed in hot tap water then PBS for 5 minutes. Slides were incubated for 10 minutes in 1X Tris Buffered Saline (TBS, Cat# BM-300, Boston BioProducts) + 0.025% Triton-X with gentle agitation. Tissue was circled on the slide with a PAP pen and incubated at 4°C overnight with rabbit anti-CD3 (Cat# ab5690, Abcam; RRID: AB_305055) and rat anti-CD8a (Cat# 14-0808-82, eBioscience; RRID: AB_2572861) primary antibodies diluted in TBS + 1% BSA in a dark humidity chamber. After overnight incubation samples were washed in PBS and gently agitated in TBS + 0.025% Triton-X for 10 minutes, then incubated for two hours at room temperature in 1:1000 anti-Rabbit IgG conjugated with Alexa Fluor 594 (Cat# A-21207, Invitrogen) and anti-rat IgG conjugated with Alexa Fluor 488 (Cat# A-21208, Invitrogen) diluted in TBS + 1% BSA. Samples were stained for 5 minutes with DAPI (10 μg/mL, Cat# D3571, Invitrogen) diluted in PBS and treated with TrueVIEW autofluorescence quenching kit (Cat# SP-8400, Vector Laboratories) according to manufacturer's protocol. Slides were coverslipped with 50 μL of Vectashield Vibrance Antifade Mounting Medium (Cat# H-1700, Vector Laboratories) and imaged within 48 hours at 40X magnification using EVOS FL Auto 2 (Invitrogen). CD3 and CD8 co-expressing cells were counted manually in 5–6 randomly selected high-powered fields from two independent tumor tissue sections.

Flow cytometry.

Blood samples were collected from submandibular (facial) veins of mice in heparin or EDTA-coated tubes. Up to 125 μL of whole blood was washed in PBS, stained with live/dead stain and then stained with surface antibodies diluted in FACS buffer (PBS with 0.1% sodium azide and 1% fetal bovine serum) for 30 minutes each at 4°C. Red blood cells were lysed with 1X BD FACS lysing solution (Cat# 349202, BD Biosciences) and processed for intracellular staining as below. Spleens were harvested from mice, weighed, and dissociated with a pestle in a 70 μm strainer in 5 mL cold RPMI. Spleen cells were lysed with 1X RBC lysis buffer (Cat #420301, BioLegend) and then resuspended in 1 mL cold RPMI for cell counting. Bone marrow was harvested from both by flushing each with 2.5 mL cold RPMI media with a 20g needle through a 70 μm strainer and resuspended in 1 mL cold RPMI for cell counting. Tumors were harvested from mice, weighed, and minced with a scalpel. Tumor pieces were then transferred to a C-tube (Miltenyi Biotec) containing 5 mL RPMI, 100 μg/mL hyaluronidase (Cat# H3506, Sigma-Aldrich) and 10 μg/mL DNase I

(Cat# 10104159001, Roche). Samples were dissociated using the 37C_m_TDK_2 program on GentleMACS Octo dissociator with heaters (Cat# 130-096-427, Miltenyi Biotec), passed through a 70 μm strainer then resuspended in 1 mL RPMI for counting. A small aliquot of each sample (1–18 μL) was stained with live/dead stain and counted using Accuri (BD Biosciences) or LUNA-FL cell counter (Logos Biosystems). 1×10^6 cells were transferred to flow tubes, washed in PBS, and stained with live/dead stain and surface antibodies diluted in FACS buffer for 30 minutes each at 4°C. After surface staining, cells were washed and fixed with FoxP3/Transcription factor staining buffer kit (Cat #00–5523, eBioscience) for 45 minutes at 4°C, then stained with anti-FoxP3 antibody overnight, and with the remaining intracellular stains for 1 hour at 4°C. Staining antibodies are listed in supplementary table S2. Following incubation, cells were washed and resuspended in 150 μL FACS buffer and stored covered at 4°C until acquisition. Single color controls were prepared with pooled cells and UltraComp eBeads compensation beads (Cat# 01-2222-41) and fluorescence-minus-one controls were prepared with pooled cells and healthy donor peripheral blood mononuclear cells for the humanized mouse study. Samples were acquired on a 5-laser Aurora flow cytometer (Cytek Biosciences) and data was analyzed using FlowJo v10 software (Tree Star; RRID: SCR_008520).

Cytokine assay.

Snap-frozen tissue was digested and homogenized in Pierce RIPA lysis and extraction buffer (Cat# 89900, Thermo Scientific) with 1X Halt Protease and Phosphatase Inhibitor cocktails (Cat# 87786 and 78420, Thermo Scientific), incubated for 30 minutes at 4°C with agitation, and sonicated at 40% amplitude for 30 seconds with pulsing (1 second on/2 seconds off). The supernatant was collected after centrifugation at 10,000*g* for 10 minutes at 4°C, and quantified using Pierce BCA Protein Assay Kit (Cat# 23225, Thermo Scientific). Protein concentrations were normalized (910 ng/mL for intracranial tumor samples, 610 ng/mL for subcutaneous tumor samples) and analyzed using multiplex immunoassays (Mouse Cytokine/Chemokine 44-Plex Discovery Assay Array, TGFB 3-Plex Discovery Assay Multi Species Array, and Mouse IFN 2-Plex Discovery Assay Array) by Eve Technologies. For each analyte, the mean concentration across biological replicates was normalized to a common scale (smallest value = minimum, largest value = maximum) and plotted as a heatmap.

Genomic DNA (gDNA) and RNA extractions from fresh frozen tissue.

Intracranial and subcutaneous mouse tumors were harvested from mice, weighed, snap frozen on dry ice and stored at −80°C before processing. Up to 35 mg of fresh frozen tissue from each tumor was mechanically dissociated using an RNAse free homogenizer in buffer RLT Plus containing 1% β-mercaptoethanol. RNA and gDNA were then extracted using the AllPrep DNA/RNA/miRNA Universal kit (Cat# 80224, QIAGEN) according to the manufacturer's guidelines. Samples were stored at −20°C until further studies. The Quant-iT PicoGreen dsDNA assay (Cat# P11496, Invitrogen) was used according to the manufacturer's protocol to quantify DNA. RNA samples were assessed for quantity and quality using Nanodrop spectrophotometer (Thermo Scientific).

Quantitative polymerase chain reaction (qPCR).

2 ug of RNA isolated from intracranial and subcutaneous mouse tumors was reverse transcribed into cDNA using High-Capacity RNA-to-cDNA Kit (Cat# 4387406, Applied Biosystems) according to manufacturer's instructions. qPCR was then performed in a 96-well plate in triplicate with 150 ng of cDNA per reaction using Applied Biosystems TaqMan Fast Advanced Master mix (Cat# 44-445-57) and Taqman gene expression assay probes (Cat# 4331182). The assay IDs for individual probes were as follows: *Gapdh* (Mm99999915_g1), *Stat1* (Mm01257286_m1), *Tap1* (Mm00443188_m1) and *B2m* (Mm00437762_m1). Amplification was according to manufacturer's protocols using the StepOnePlus real-time PCR system (Cat# 4376600, Applied Biosystems). Fold change in gene expression relative to controls was calculated using the delta-delta Ct method.

TCR sequencing and analysis.

The Adaptive Biotechnologies immunoSEQ mouse T cell receptor beta (mmTCRB) service was used to identify and quantify the frequency of specific T cell clones present in tumors. DNA from fresh frozen intracranial and extracranial mouse tumors was diluted to 83 ng/ul and shipped on dry ice to Adaptive Biotechnologies for TCR sequencing services. Data was analyzed using immunoSEQ Analyzer software (Analyses 3.0; Adaptive Biotechnologies).

Statistical analyses.

Statistical analyses performed are described in the figure legend for each experiment. Results are presented as mean ± standard error of means (SEM). Comparisons involving multiple groups were performed using one-way analysis of variance (ANOVA) with Tukey or Dunnett's multiple comparison tests. GraphPad Prism v.9 (RRID: SCR_002798) was used for all statistical analyses and p values < 0.05 were considered statistically significant.

Data availability.

TCR sequencing data from the immunoSEQ assay is available through the immuneACCESS portal (https://doi.org/10.21417/NN2023CCR). Representative and processed data are presented within this article and its supplementary materials. All other reasonable data including more detailed methods and materials (eg. cell line constructs) generated in this study can be made available upon request from the corresponding author.

RESULTS

CDKi sensitizes intracranial tumors to PD-1 inhibition in preclinical models of CDK-mutant melanoma brain metastasis

We evaluated intracranial and extracranial response to single- and dual-agent ICI targeting PD-1 and CTLA4 in transplantable dual extracranial/intracranial models of melanoma brain metastasis (24–26). We found that YUMM1.7, a melanoma line derived from $Braf^{V600E}Cdkn2a^{-/-}Pten^{-/-}$ mice (27), exhibited resistance to single agent anti-PD-1 in both tumor locations in mice bearing dual subcutaneous/intracranial YUMM1.7 tumors (Fig. 1A−B). We also observed intracranial resistance to single-agent anti-CTLA-4 and very limited sensitivity to dual-agent ICI despite extracranial sensitivity to both treatments

(Fig. 1A−B). We used this model to investigate the role of CDKi in potentiating anti-tumor immune responses and sensitizing intracranial metastases to PD-1 inhibition.

In mice with intracranial and subcutaneous YUMM1.7 tumors, abemaciclib treatment resulted in improved overall survival (dependent on intracranial tumor growth) and decreased subcutaneous tumor growth (Fig. S1A, Fig. 1C−D). However, systemic depletion of $CD8^+$ T cells abrogated the therapeutic benefit, suggesting a role for cytotoxic T cell mediated intracranial and extracranial tumor control following abemaciclib treatment (Fig. 1C−D, S1B).

Next, we investigated whether CDKi can sensitize intracranial tumors to PD-1 inhibition using a phased combination strategy with ICI lead-in, which was previously shown to have the greatest efficacy (11), in mice bearing dual subcutaneous/intracranial YUMM1.7 tumors (Fig. 1E). Based on bioluminescence imaging (BLI) of luciferase-tagged intracranial tumors, the change in intracranial tumor burden was significantly lower with combination abemaciclib and anti-PD-1 ("combination therapy") (Fig. 1F). Overall survival improved with anti-PD-1 monotherapy (median survival 35 days vs 29 days in controls) – likely due to luciferase expression in tumor cells, which can elicit an anti-tumor immune response in immunocompetent mouse models (28) – as well as with abemaciclib monotherapy (median survival 33.5 days) (Fig. 1G). However, combination therapy resulted in the greatest intracranial efficacy (median survival 44 days; Fig. 1G). Complete regression of intracranial tumors was observed in 1 out of 6 animals treated with anti-PD-1 (17%) and 5 out of 6 animals treated with combination therapy (83%) (Fig S1C−D). We did not observe any added benefit from combination therapy extracranially; subcutaneous tumor growth was equally inhibited with abemaciclib monotherapy and combination therapy compared to control mice (Fig. 1H).

Next, we evaluated efficacy of combination CDKi and anti-PD-1 in the aggressive B16-F10 melanoma model. B16-F10 tumors harbor *Cdkn2a* loss, are poorly immunogenic and thus immunologically cold, and are resistant to single-agent ICI (29,30) (Fig. 1I, Fig. S1E). Tumors were implanted subcutaneously then intracranially and treated as described above (Fig. 1E). Intracranial and subcutaneous B16-F10 tumors were resistant to PD-1 inhibition, as expected, as well as abemaciclib monotherapy (Fig. 1J−K). Despite tumor resistance to both monotherapies, combination therapy improved overall survival (dependent on intracranial tumor growth; median survival 19 days vs 16 days with control) and reduced subcutaneous tumor growth (Fig. 1J−K). Taken together, these data indicate that combination CDKi and PD-1 inhibition can sensitize intracranial and extracranial melanoma, reducing tumor growth and improving overall survival.

Combination CDK4/6 and PD-1 inhibition reduces tumor burden in preclinical model of breast cancer brain metastasis

Triple-negative breast cancers (TNBCs) lack effective therapies. They are commonly treated with ICI with mixed efficacy and are often resistant to single-agent CDKi (14,31,32). We asked whether combination therapy can sensitize a TNBC model of brain metastasis with dual mammary/intracranial 4T1 tumors implanted into syngeneic BALB/c mice (33) (Fig. 2A). BLI revealed a significantly lower intracranial tumor burden with combination therapy

compared to controls and abemaciclib monotherapy groups (Fig. 2B). Mammary tumor mass, measured at survival endpoint, was significantly reduced with combination therapy compared to controls and anti-PD-1 treated groups (Fig. 2C). Despite lower tumor burden with combination treatment, we did not find any differences in overall survival between treatment groups in this model (Fig. 2D). Instead, we observed significant weight loss in mice receiving daily abemaciclib treatments relative to vehicle-treated mice, suggesting greater drug-related toxicity in this mouse strain (Fig. 2E, S2A). Abemaciclib treatment in C57BL/6 mice produced a transient drop in body weights but the mice recovered after a few days despite daily dosing (Fig. S2B). Overall, combination therapy reduced intracranial and extracranial growth of 4T1 tumors compared to control-treated mice but did not extend survival.

Combination CDK4/6 and PD-1 inhibition drives anti-tumor inflammation into ICI resistant intracranial tumors

We investigated inflammatory response to single-agent and combination CDKi and PD-1 inhibition in intracranial tumors. First, we quantified $CD8^+$ T cell densities in intracranial YUMM1.7, B16-F10 and 4T1 tumors collected at survival endpoint using immunofluorescence staining. We observed an increase in $CD8^+$ T cell density in intracranial YUMM1.7 tumors treated with single-agent anti-PD-1 compared to controls, while combination therapy increased tumor infiltration by $CD8^+$ T cells compared to controls and abemaciclib monotherapy (Fig. 3A). In the immunologically cold B16-F10 tumors, combination therapy resulted in a statistically significant increase in intracranial tumor infiltrating $CD8^+$ T cells relative to control and abemaciclib monotherapy arms (Fig. 3B). Lastly, compared to control 4T1 tumors, intracranial $CD8^+$ T cell densities were unchanged with anti-PD-1 treatment alone, increased with abemaciclib monotherapy, and highest in tumors from mice treated with combination therapy (Fig. 3C). Although insufficient subcutaneous YUMM1.7 tumor tissue was available for statistical analysis, an increase in $CD8^+$ T cells similar to intracranial tumors was observed in subcutaneous B16-F10 tumors treated with combination therapy (Fig. 3D−E). Mammary 4T1 tumors demonstrated a similar trend of increased $CD8^+$ T cell densities with treatment as their matched intracranial tumors although the results did not reach significance (Fig. 3F).

Multiplex immunoassays revealed that intracranial YUMM1.7 tumors treated with abemaciclib alone (daily for 8 days starting on d8) or in combination with anti-PD-1 (4 doses starting on d5) had lower concentrations of anti-inflammatory and T_H1-suppressive cytokines such as IL4, IL10 and TGF-β (34–36) (Fig. S2C). Expression of these cytokines was also reduced with abemaciclib treatment, but not combination therapy, in subcutaneous tumors (Fig. S2D). Several chemokines implicated in recruitment of immunosuppressive cell types (such as CCL12 and CCL21) and pleiotropic cytokines with mixed pro- and anti-inflammatory effects (such as LIF, IL-6 and IL-11) were similarly reduced with abemaciclib monotherapy or combination therapy in intracranial tumors and with abemaciclib alone in subcutaneous tumors (34–36) (Fig. S2C−D). Chemokines that can recruit T_{REG} cells were expressed at lower levels in intracranial tumors treated with anti-PD-1 or combination therapy, and in subcutaneous tumors treated with anti-PD-1 (Fig. S2C−D). Importantly, several pro-inflammatory and T_H1-associated cytokines, including TNFα, IFNγ and IL-2,

were lower in anti-PD-1 treated intracranial and subcutaneous tumors, but elevated with either abemaciclib monotherapy or combination therapy in both tumor sites (Fig. S2C−D).

Together, these results indicate that combination CDKi and PD-1 inhibition can drive cytotoxic T cell infiltration into both intracranial and subcutaneous tumors. In intracranial tumors, combination therapy can reduce expression of immunosuppressive cytokines, especially those that inhibit T_H1-type responses or recruit T_{REG} cells, while increasing pro-inflammatory and T_H1-associated cytokines.

Combination CDK4/6 and PD-1 inhibition increases tumor immunogenicity in an organ-specific manner

We performed flow cytometry on YUMM1.7 tumors to characterize treatment-related changes within the tumor microenvironment that confer survival benefit (Fig. 4A, Fig. S3A). Intracranial tumors collected mid-treatment were of comparable size across all treatment groups, while subcutaneous tumor burden was lower in mice receiving combination therapy (Fig. 4B). Previous studies have shown that CDKi reduces proliferation and increases antigen presentation and PD-L1 expression in tumor cells (19,22,37). We observed decreased Ki-67 expression by $CD45^-$ cells in subcutaneous tumors treated with abemaciclib or combination therapy relative to control treatment and anti-PD-1 monotherapy but not in intracranial tumors (Fig. 4C). Overall, Ki-67 expression was significantly lower in intracranial tumors relative to their matched extracranial tumors ($p<0.0001$ for control-treated intracranial vs subcutaneous tumors), which may account for the lack of CDKi-mediated decrease in tumor cell proliferation intracranially. PD-L1 expression in $CD45^-$ cells was higher in intracranial tumors relative to subcutaneous tumors ($p<0.0001$ for control-treated intracranial vs subcutaneous tumors; Fig. 4D). Consistent with previous studies, PD-L1 expression was upregulated with abemaciclib and combination treatment in subcutaneous YUMM1.7 tumors (Fig. 4D). However, in intracranial tumors, PD-L1 expression was elevated following single-agent anti-PD-1 or combination therapy, indicating that distinct mechanisms regulate tumor cell PD-L1 expression in distinct anatomical locations (Fig. 4D). We used expression of B2M, a component of major histocompatibility complex (MHC) class I, to measure antigen presentation by tumor cells. The proportion of B2M+ cells did not change with treatment in intracranial tumors and was lower in subcutaneous tumors treated with abemaciclib and combination therapy (Fig. 4E). However, average B2M expression by CD45− cells increased with anti-PD-1 alone or in combination with abemaciclib in intracranial tumors (Fig. 4F). The proportion of tumor cells expressing MHC class II was similarly decreased with abemaciclib and combination therapy in subcutaneous tumors, and was lower with abemaciclib monotherapy (relative to other treatment groups) in intracranial tumors (Fig. 4G).

We performed similar characterization of intracranial and subcutaneous B16-F10 tumors (Fig. S4A). Tumors collected earlier in treatment were equivalent in size across treatment arms and no difference in proliferation of $CD45^-$ cells was observed (Fig. S4B−C). PD-L1 expression on B16-F10 tumor cells was equivalent in both tumor locations (similar to subcutaneous YUMM1.7 tumors) and did not change with treatment (Fig. S4D). B16-F10 tumors are poorly immunogenic with very low MHC class I expression relative to

YUMM1.7 tumor cells (Fig. 4E−F, Fig. S4E−F). However, we observed a trend towards higher percentage of B2M-expressing $CD45^-$ cells in intracranial tumors treated with combination therapy relative to control or anti-PD-1 monotherapy (Fig. S4E). Overall B2M expression by $CD45^-$ cells was significantly higher in intracranial tumors treated with abemaciclib relative to control and with combination therapy relative to control or anti-PD-1 alone (Fig. S4F). No significant differences were noted in subcutaneous B16-F10 tumors (Fig. S4E−F). MHC class II expression did not change with treatment in either tumor location (Fig. S4G).

To further explore changes in immunogenicity of tumor cells, we quantified *B2m* (antigen presentation), *Tap1* (antigen processing) and *Stat1* (interferon signaling) gene expression in intracranial and subcutaneous YUMM1.7 tumors harvested on d16 (Fig. 4A). Consistent with previously reports in extracranial tumor models, all 3 genes were strongly upregulated in intracranial YUMM1.7 tumors following treatment with abemaciclib as well as combination therapy, while PD-1 inhibition resulted in increased expression of *B2m* and *Stat1* (19,21) (Fig. 4H). No significant changes were observed in subcutaneous tumors at this timepoint (Fig. 4I).

Taken together, these data indicate differential response to treatment in the intracranial and extracranial tumor compartments. Consistent with previous reports, we found decreased proliferation and increased PD-L1 expression only in immunogenic extracranial tumors following treatment with abemaciclib alone or in combination with anti-PD-1. While we did not find similar changes in matched intracranial tumors, we observed increased antigen presentation with combination treatment in intracranial tumors regardless of their baseline immunogenicity.

CDKi and combination therapy remodels the tumor immune microenvironment

To understand how CDK4/6 and PD-1 inhibition enhance anti-tumor immunity, we evaluated the immune component of intracranial and subcutaneous YUMM1.7 tumors (Fig. S3A). We observed slightly elevated immune infiltration into intracranial, but not subcutaneous, tumors with PD-1 inhibition relative to controls (Fig. 5A). No changes in overall proportion of T cells were observed at this timepoint (Fig. S5A). However, ratio of $CD8^+$:$CD4^+$ T cells was elevated with abemaciclib therapy among both intracranial and subcutaneous YUMM1.7 tumors (Fig. 5B). In intracranial tumors, $CD8^+$ T cell proliferation ($Ki\text{-}67^+$) increased with combination therapy, specifically among $CD44^+CD62L^-$ effector memory (T_{EM}) and $CD44^-CD62L^-$ pre-effector-like subsets (Fig. 5C, Fig. S5B−C). As a result, $CD8^+$ pre-effector-like cells, while rare, were more abundant in tumors treated with combination therapy relative to control group (Fig. 5D). Pre-effector-like $CD8^+$ cells differentiate into T_{EM} cells, and together these subsets exhibit the greatest capacity for tumor rejection and enhance efficacy of PD-1 blockade (38). Expression of cytolytic enzyme granzyme B in $CD8^+$ T cells was also greatly enhanced with combination therapy in both intracranial and subcutaneous tumors (Fig. 5E). While we did not discover any significant changes in conventional $CD4^+$ T cells, immunosuppressive T_{REG} ($CD4^+CD25^+FOXP3^+$) cells decreased in intracranial tumors with all treatments, and were lowest with combination therapy (Fig. 5F). We also observed a trend towards reduced T_{REG} cell percentages, and

a significant reduction in proliferation of T_{REG} cells, in subcutaneous tumors treated with abemaciclib and combination therapy (Fig. 5F, Fig S5D). The proportion of $CD4^+$, but not $CD8^+$, T cells co-expressing PD-1 and TIM3 – a marker of T cell dysfunction – decreased following anti-PD-1 and combination therapy in intracranial tumors, with a similar trend observed in subcutaneous tumors (Fig. 5G−H). Notably, we found a higher percentage of $PD\text{-}1^+TIM3^+$ T cells in intracranial tumors compared to their matched subcutaneous tumors (p=0.005 for $CD4^+$ and p=0.02 for $CD8^+$ T cells among controls; Fig. 5G−H).

Treatment-induced changes among additional lymphocytic and myeloid infiltrates varied by tumor location. In subcutaneous tumors, proportion of B cells ($CD19^+$) present was significantly lower with combination therapy, with a similar trend seen in intracranial tumors, while PD-1 inhibition increased B cell proliferation intracranially (Fig. S5E−F). Polymorphonuclear myeloid-derived suppressor cells (PMN-MDSCs) and neutrophils ($CD11b^+Ly6G^+$) were more common in control subcutaneous tumors compared to intracranial tumors (p=0.002; Fig. S5G). Subcutaneous tumors treated with abemaciclib or combination therapy had a lower proportion of PMN-MDSCs/neutrophils as well as monocytic-MDSCs (M-MDSCs) and monocytes ($CD11b^+Ly6G^-Ly6C^+$) compared to anti-PD-1 treated tumors (Fig. S5G−H). Although overall proportion of macrophages ($CD11b^+F4/80^+$) did not change significantly with treatment in either tumor location, we observed a higher ratio of $CD206^-iNOS^+$ M1-like macrophages to $CD206^+iNOS^-$ M2-like macrophages in vehicle-treated subcutaneous tumors compared to intracranial tumors (p<0.0001 for control-treated intracranial vs subcutaneous tumors; Fig. S5I−J). This M1-like:M2-like ratio was reduced with abemaciclib and combination therapy in subcutaneous tumors, indicating a shift from pro-inflammatory to anti-inflammatory macrophages (Fig. S5J).

Surface expression of PD-L1 on tumor immune infiltrates also increased with treatment in a cell type and location-dependent manner. PD-L1 expressing proportions of $CD45^+$ cells, and especially myeloid subsets, were elevated in intracranial tumors with PD-1 inhibition, alone and in combination with abemaciclib, and in subcutaneous tumors with abemaciclib, alone and in combination with anti-PD-1 (Fig. S6A−E). Treatment effect on lymphocytes was not location-dependent, with B cells and natural killer (NK) cells upregulating PD-L1 similarly in both tumor compartments following combination therapy (Fig. S6F−G).

Characterization of immune infiltrates among poorly immunogenic B16-F10 tumors revealed distinct effects of CDKi and PD-1 inhibition on the TIME relative to YUMM1.7 tumors. As expected, the overall proportion of $CD45^+$ cells in intracranial and subcutaneous B16-F10 tumors was significantly lower than YUMM1.7 tumors (4.1% vs 48.7% in intracranial and 12.8% vs 66.0% in subcutaneous B16-F10 vs YUMM1.7 tumors, respectively; p<0.0001 for both; Fig. 5A, Fig. S7A). As in YUMM1.7 tumors, there were no significant changes in immune infiltration of B16-F10 tumors with any treatment, however abemaciclib treated subcutaneous tumors had a significantly higher proportion of $CD45^+$ cells compared to their matched intracranial tumors suggesting the presence of an inflammatory response extracranially (Fig. S7A). T cell infiltration into B16-F10 tumors was limited, with more $CD4^+$ than $CD8^+$ T cells and this ratio did not change with abemaciclib or combination therapy in either location (Fig. S7C). Importantly, abemaciclib

monotherapy reduced proliferation of both $CD4^+$ and $CD8^+$ T cells, especially $CD8^+$ T_{EM} cells, in intracranial tumors relative to controls or anti-PD-1 monotherapy (Fig. S7D−F). A similar but less pronounced decrease in T cell proliferation was also observed in intracranial tumors treated with combination therapy (Fig. S7D−F). T_{REG} cell proliferation, on the other hand, did not change significantly with any treatment relative to controls, although anti-PD-1-treated intracranial tumors had more $Ki67^+$ T_{REG} cells compared to combination therapy group (Fig. S7G). We observed a trend towards fewer T_{REG} cells present in subcutaneous tumors treated with abemaciclib or combination therapy (Fig. S7H). Notably, abemaciclib monotherapy in intracranial tumors and combination therapy in subcutaneous tumors reduced $PD1^+TIM3^+$ proportion of both $CD4^+$ and $CD8^+$ T cells relative to control or anti-PD-1 groups, suggesting less exhausted T cell phenotypes (Fig. S7I−J). Unlike in YUMM1.7 tumors, no significant treatment-induced changes in proportion of B cells were observed among B16-F10 tumors, although abemaciclib and combination therapy reduced B cell proliferation in intracranial tumors (Fig. S8A−B). Similarly, no significant changes were observed among myeloid cells aside from decreased ratio of M1-like to M2-like macrophages in intracranial tumors treated with abemaciclib or combination therapy (Fig. S8C−F). Finally, we did not observe any changes in surface PD-L1 expression among immune cells overall, however PD-L1 expression on intracranial tumor-infiltrating B cells increased with all treatments relative to controls (Fig. S8G−H).

Taken together, our findings highlight differences between the intracranial and extracranial microenvironments. The results described above indicate that combined CDK4/6 and PD-1 inhibition remodels the TIME in a location-specific manner and supports $CD8^+$ T cell mediated anti-tumor immunity in immunogenic tumors through recruitment and expansion of effector subsets coupled with depletion of immunosuppressive T_{REG} cells. In poorly immunogenic tumors, although CDKi reduced proliferation of B and T cells, lower proportions of T_{REG} and exhausted effector T cells may be responsible for enhanced tumor control observed with combined CDK4/6 and PD-1 inhibition.

CDKi and combination therapy associated with increased extracranial priming and clonal expansion of T cells

We further explored how CDKi and anti-PD-1, alone or in combination, affect early adaptive immune responses by evaluating T cell receptor (TCR) repertoires of intracranial and subcutaneous YUMM1.7 tumors treated as before (Fig. 4A). In intracranial tumors, no treatment-related changes were observed in the total number of productive templates, which represent TCRβ sequences that code for a functional peptide (Fig. S9A). In subcutaneous tumors, we detected more productive TCR templates with abemaciclib treatment compared to control or anti-PD-1, or compared to their matched intracranial tumors (Fig. S9A). The number of unique productive TCR rearrangements, which demonstrates the breadth of the TCR repertoire, was elevated in subcutaneous tumors treated with abemaciclib, and a similar trend was observed with combination therapy, relative to control or anti-PD-1 treatments (Fig. S9B). Additionally, we detected more unique productive TCR rearrangements with abemaciclib and combination treatment in extracranial tumors compared to matched intracranial tumors, indicating a broadening of the TCR repertoire in the extracranial compartment (Fig. S9B). Subcutaneous tumors were more polyclonal (higher sample

clonality score) than intracranial tumors when treated with single-agent anti-PD-1 or combination therapy, with a similar trend seen in abemaciclib-treated tumors (Fig. S9C). Morisita indices were calculated to evaluate TCR overlap between tumors (39). We observed considerable TCR overlap between matched intracranial and subcutaneous tumors across all groups, but very little TCR overlap between individual animals, highlighting the distinct TCR repertoire of each mouse (Fig. S10A).

Overall, we did not find any treatment-induced changes in the intracranial TCR repertoires, but in extracranial tumors frequency of T cells was higher with abemaciclib treatment and richness of the intratumoral TCR repertoire was elevated with abemaciclib and combination therapy. This suggests that CDKi facilitates T cell priming in the extracranial compartment.

CDKi supports T cell development and depletes T_{REG} cells in humanized mouse models

To better understand the effects of CDKi on the immune system, we investigated the effect of abemaciclib on human T cell proliferation, activation and maintenance in NSG mice engrafted with human $CD34^+$ hematopoietic stem cells (Fig. 6A, Fig. S11A). Flow cytometric analysis revealed a drop in human $CD45^+$ ($hCD45^+$) cell fraction in peripheral blood and bone marrow (BM), and significant splenic contraction without a shift in hCD45 proportion, after 2 weeks of daily abemaciclib (Fig. 6B−C; Fig. S12A−C). Proliferation of human immune cells was unaffected in BM and peripheral blood but reduced in the spleen with abemaciclib (Fig. 6D; Fig. S12D−E). Proliferation of lymphocytes was reduced in BM and spleen, but unaffected in peripheral blood, after 2 weeks of abemaciclib treatment (Fig. S12F−K). Despite reduced proliferation, the proportion of $hCD45^+$ cells comprised of T cells, including both $CD8^+$ and $CD4^+$ T cells, increased with abemaciclib in peripheral blood, and $CD8^+$ T cells were similarly elevated in the spleen (Fig. 6E−G; Fig S12L). Conversely, $CD4^+$ T_{REG} cells ($CD4^+CD127^-CD25^+FOXP3^+$) were decreased in proportion in peripheral blood and spleen and exhibited reduced proliferative capacity in the blood (Fig. 6H−J). As a result, abemaciclib treatment increased the ratio of $CD8^+$ to regulatory T cells in peripheral blood and spleen (Fig. S12M−N). This suggests a supportive role for CDKi in proliferation and maintenance of $CD8^+$ cells and a negative effect on T_{REG} cells.

Upon closer examination of activation status, we observed an increase in $hCD45^+$ proportion of naïve ($CCR7^+CD45RA^+$; T_N) $CD8^+$ T cells in blood and spleen (Fig. 6K−L). In contrast, $CD8^+$ T_{EM} subset ($CCR7^-CD45RA^-$) was expanded in peripheral blood from vehicle-treated mice (Fig. 6K). Consistent with an expanded T_N population in abemaciclib treated mice, we found fewer $CD8^+$ T cells expressing Eomes, a master regulator of $CD8^+$ T_{EM} and T_{CM} cells, and CD38, a marker of activation, as well as reduced expression of costimulatory receptor CD28, in $CD8^+$ T cells across all compartments (Fig. 6M; Fig. S12O−V). Proportion of $CD8^+$ T cells expressing granzyme B and exhaustion markers TIGIT and PD-1 was also lower with abemaciclib treatment in all immune compartments (Fig. 6N−P; Fig. S12W−AB). Similar but less pronounced phenotypic changes were observed in $CD4^+$ T cells with abemaciclib treatment. CD4+ T_N subset was significantly expanded in peripheral blood but not in the spleen (Fig. S13A, Fig. 6L). Fewer CD4+ T cells were found to express CD38 in BM and spleen, and expression of CD28 was reduced across all compartments (Fig. S13B−G). Proportion of $CD4^+$ T cells expressing PD-1 remain

unchanged but TIGIT$^+$ proportion was lower in blood and spleens of abemaciclib treated mice (Fig. S13H−M). Collectively, these data suggest that treatment with abemaciclib can inhibit lymphocyte proliferation and specifically deplete regulatory T cells as previously reported (19,40), but also plays a supportive role in development and maturation of CD4$^+$ and CD8$^+$ T cells.

DISCUSSION

Given the poor prognosis associated with brain metastases, there is a critical need for therapeutic strategies that augment anti-tumor immunity and produce durable regression of intracranial metastases. In this study, we showed that combination CDKi and PD-1 inhibition resulted in reduced tumor burden in pre-clinical immunocompetent models of brain metastasis and improved overall survival in the melanoma brain metastasis models. Enhanced control of intracranial tumors was attributable to a less immunosuppressive TIME coupled with increased immunogenicity and cytotoxic T cell infiltration of intracranial tumors. Given the frequency of CDK4/6 pathway alterations in brain metastases (9,10), our findings indicate that exploiting this genetic vulnerability in tandem with immunotherapy is a promising approach for improving intracranial disease control.

CDK4/6 dysregulation has been implicated in cancer immune evasion, orchestrating an immunologically cold tumor microenvironment and circumventing immune-mediated tumor cell senescence (11,41). As a result, CDK4/6 dysregulation is associated with poor response to PD-1 blockade in some cancers (12,13). Conversely, the link between CDKi and anti-tumor immunity has been described in extracranial tumors. CDKi can enhance tumor immunogenicity by increasing antigen presentation and activating interferon response pathways in extracranial tumors (19,21,42). In our dual extracranial/intracranial model of melanoma brain metastasis, we observed similar changes in intracranial, but not subcutaneous, YUMM1.7 tumors following abemaciclib treatment, consistent with the improved intracranial, but not extracranial, efficacy of combined abemaciclib and anti-PD-1 relative to abemaciclib monotherapy in the YUMM1.7 model. CDKi also acts on T cells, suppressing T_{REG} proliferation while enhancing activation of antigen-experienced T cells (19,20). We observed reduced intratumoral frequencies and proliferation of T_{REG} cells with abemaciclib and combination treatment, and similar effects were observed in tumor-free humanized mice. CD8$^+$ effector subsets proliferated at a higher rate in intracranial YUMM1.7 tumors treated with combination therapy, consistent with the enhanced disease control. In humanized mice, we observed reduced T cell dysfunction with abemaciclib administration, and similarly, reduced expression of co-inhibitory receptors on intratumoral CD4$^+$ and CD8$^+$ T cells was associated with treatment efficacy in poorly immunogenic B16-F10 tumors. Importantly, CDKi can reportedly increase PD-L1 expression on tumor cells by stabilizing membranous localization of the protein, leading to immune escape (22). We observed varied, location-dependent changes in tumor cell PD-L1 expression with treatment. Our findings highlight the distinct microenvironments of intracranial and extracranial tumors. These microenvironmental differences, together with baseline immunogenicity of the cancer cells, likely drive discordant treatment responses in intracranial and extracranial compartments, necessitating evaluation of intracranial efficacy of novel treatment strategies as we have done in this study.

We observed sustained weight loss in BALB/c mice, and transient weight loss in C57BL/6 mice, with daily abemaciclib dosed at 90 mg/kg, indicating some drug-related toxicity. However, irAEs are uncommon in the wildtype mouse strains therefore we did not detect irAEs with dual-agent ICI, which can be toxic in patients, or with combination abemaciclib and anti-PD-1 treatment. Recent phase I studies discovered significant toxicity with abemaciclib and the anti-PD-1 agent pembrolizumab in patients (43,44). The combination of palbociclib and pembrolizumab is relatively well-tolerated, however, and is currently being investigated for patients with extracranial metastases (45); this suggests different drug-specific toxicity profiles with the combination therapy. The current safety profile does not support the use of abemaciclib with anti-PD-1 outside of a clinical trial and these combinations should be carefully evaluated in patients with brain metastases, including determining the appropriate CDKi and anti-PD-1 agents and dosages.

In addition to safety concerns, the translational potential of our findings hinges on identification of the patient population most likely to benefit from combination CDKi and ICI and optimization of dosing regimens. In this study, we established efficacy of CDKi and anti-PD-1 in intracranial metastases with *Cdkn2a* loss. However, data suggests that genomic alterations in the CDK4/6 pathway may have differential sensitivity to CDKi (46), and in the absence of these genomic alterations, CDK4/6 pathway can be activated as a result of cyclin D1 upregulation downstream of aberrant mitogenic signaling (eg. hormone receptor, PI3K/AKT and MAPK signaling pathways) or epigenetic silencing of *CDKN2A* (11,47–50). Importantly, clinical benefit of combined CDK4/6 and PD-1 inhibition has been observed in advanced hormone receptor-positive breast cancers and *KRAS*-mutant lung cancers in the extracranial setting (43–45). Additional studies are therefore needed to determine which histologic and genetic features are associated with response to combination CDKi and ICI. Moreover, the pre-clinical models used in our study involve concurrent extracranial and intracranial tumors to mimic immune responses in brain metastasis patients, which differ from those seen in primary brain tumor patients. The presence of extracranial tumors, however, obscures whether combination CDKi and ICI would be equally effective in patients with intracranial metastases in the absence of active extracranial disease, a translationally relevant question that should be investigated in future studies. Lastly, the phased combination approach with ICI lead-in that we employed in our studies was shown to be most effective in pre-clinical models (11). Human studies thus far have only tested safety and efficacy of co-administering CDK4/6 and PD-1 inhibitors (43–45). Optimal scheduling and dosing of drugs will need to be determined in patients with brain metastases. A clinical trial is now planned to evaluate the efficacy and toxicity of the combination of CDKi and ICI for patients with brain metastases.

Supplementary Material

Refer to Web version on PubMed Central for supplementary material.

ACKNOWLEDGMENTS

Funding for this work was provided by Eli Lilly. PKB was also supported by the Breast Cancer Research Foundation (ELFF-17), the Demetra Fund of the Hellenic Women’s Association, Terry and Jean de Gunzburg

MGH Research Scholar Award and the NIH (5R01CA227156-02). MAB was supported by NIH (R24 OD026440). Figures were created with BioRender.com.

Authors' disclosures: Outside the scope of this work, P.K.B. has consulted for Angiochem, Genentech-Roche, Lilly, Tesaro, ElevateBio, Pfizer, SK Life Sciences, Advice Connect Inspire, MPM, Axiom and Dantari, received institutional grant/research support (to MGH) from Merck, BMS, and Mirati and honoraria from Merck, Genentech-Roche, Pfizer and Lilly.

REFERENCES

1. Alexander W The Checkpoint Immunotherapy Revolution: What Started as a Trickle Has Become a Flood, Despite Some Daunting Adverse Effects; New Drugs, Indications, and Combinations Continue to Emerge. P T 2016;41:185–91 [PubMed: 26957887]
2. Long GV, Atkinson V, Lo S, Sandhu S, Guminski AD, Brown MP, et al. Combination nivolumab and ipilimumab or nivolumab alone in melanoma brain metastases: a multicentre randomised phase 2 study. Lancet Oncol 2018;19:672–81 [PubMed: 29602646]
3. Tawbi HA, Forsyth PA, Hodi FS, Lao CD, Moschos SJ, Hamid O, et al. Safety and efficacy of the combination of nivolumab plus ipilimumab in patients with melanoma and asymptomatic or symptomatic brain metastases (CheckMate 204). Neuro Oncol 2021;23:1961–73 [PubMed: 33880555]
4. Brastianos PK, Lee EQ, Cohen JV, Tolaney SM, Lin NU, Wang N, et al. Single-arm, open-label phase 2 trial of pembrolizumab in patients with leptomeningeal carcinomatosis. Nat Med 2020;26:1280–4 [PubMed: 32483359]
5. Kim R, Keam B, Kim S, Kim M, Kim SH, Kim JW, et al. Differences in tumor microenvironments between primary lung tumors and brain metastases in lung cancer patients: therapeutic implications for immune checkpoint inhibitors. BMC Cancer 2019;19:19 [PubMed: 30616523]
6. Tawbi HA, Forsyth PA, Algazi A, Hamid O, Hodi FS, Moschos SJ, et al. Combined Nivolumab and Ipilimumab in Melanoma Metastatic to the Brain. N Engl J Med 2018;379:722–30 [PubMed: 30134131]
7. Curtin JA, Fridlyand J, Kageshita T, Patel HN, Busam KJ, Kutzner H, et al. Distinct sets of genetic alterations in melanoma. N Engl J Med 2005;353:2135–47 [PubMed: 16291983]
8. Walker GJ, Flores JF, Glendening JM, Lin A, Markl IDC, Fountain JW. Virtually 100% of melanoma cell lines harbor alterations at the DNA level withinCDKN2A, CDKN2B, or one of their downstream targets. Genes, Chromosomes and Cancer 1998;22:157–63 [PubMed: 9598804]
9. Brastianos PK, Carter SL, Santagata S, Cahill DP, Taylor-Weiner A, Jones RT, et al. Genomic Characterization of Brain Metastases Reveals Branched Evolution and Potential Therapeutic Targets. Cancer Discov 2015;5:1164–77 [PubMed: 26410082]
10. Shih DJH, Nayyar N, Bihun I, Dagogo-Jack I, Gill CM, Aquilanti E, et al. Genomic characterization of human brain metastases identifies drivers of metastatic lung adenocarcinoma. Nat Genet 2020;52:371–7 [PubMed: 32203465]
11. Jerby-Arnon L, Shah P, Cuoco MS, Rodman C, Su MJ, Melms JC, et al. A Cancer Cell Program Promotes T Cell Exclusion and Resistance to Checkpoint Blockade. Cell 2018;175:984–97 e24 [PubMed: 30388455]
12. Ebot EM, Duncan DL, Tolba K, Fabrizio D, Frampton GM, Comment LA, et al. Deletions on 9p21 are associated with worse outcomes after anti-PD-1/PD-L1 monotherapy but not chemoimmunotherapy. NPJ Precis Oncol 2022;6:44 [PubMed: 35739333]
13. Zhao X, Cohen EEW, William WN Jr., Bianchi JJ, Abraham JP, Magee D, et al. Somatic 9p24.1 alterations in HPV(−) head and neck squamous cancer dictate immune microenvironment and anti-PD-1 checkpoint inhibitor activity. Proc Natl Acad Sci U S A 2022;119:e2213835119 [PubMed: 36395141]
14. Niu Y, Xu J, Sun T. Cyclin-Dependent Kinases 4/6 Inhibitors in Breast Cancer: Current Status, Resistance, and Combination Strategies. J Cancer 2019;10:5504–17 [PubMed: 31632494]
15. Brastianos PK, Kim AE, Wang N, Lee EQ, Ligibel J, Cohen JV, et al. Palbociclib demonstrates intracranial activity in progressive brain metastases harboring cyclin-dependent kinase pathway alterations. Nat Cancer 2021;2:498–502 [PubMed: 35122016]

16. Tolaney SM, Sahebjam S, Le Rhun E, Bachelot T, Kabos P, Awada A, et al. A Phase II Study of Abemaciclib in Patients with Brain Metastases Secondary to Hormone Receptor-Positive Breast Cancer. Clin Cancer Res 2020;26:5310–9 [PubMed: 32694159]

17. Raub TJ, Wishart GN, Kulanthaivel P, Staton BA, Ajamie RT, Sawada GA, et al. Brain Exposure of Two Selective Dual CDK4 and CDK6 Inhibitors and the Antitumor Activity of CDK4 and CDK6 Inhibition in Combination with Temozolomide in an Intracranial Glioblastoma Xenograft. Drug Metab Dispos 2015;43:1360–71 [PubMed: 26149830]

18. Patnaik A, Rosen LS, Tolaney SM, Tolcher AW, Goldman JW, Gandhi L, et al. Efficacy and Safety of Abemaciclib, an Inhibitor of CDK4 and CDK6, for Patients with Breast Cancer, Non-Small Cell Lung Cancer, and Other Solid Tumors. Cancer Discov 2016;6:740–53 [PubMed: 27217383]

19. Goel S, DeCristo MJ, Watt AC, BrinJones H, Sceneay J, Li BB, et al. CDK4/6 inhibition triggers anti-tumour immunity. Nature 2017;548:471–5 [PubMed: 28813415]

20. Deng J, Wang ES, Jenkins RW, Li S, Dries R, Yates K, et al. CDK4/6 Inhibition Augments Antitumor Immunity by Enhancing T-cell Activation. Cancer Discov 2018;8:216–33 [PubMed: 29101163]

21. Schaer DA, Beckmann RP, Dempsey JA, Huber L, Forest A, Amaladas N, et al. The CDK4/6 Inhibitor Abemaciclib Induces a T Cell Inflamed Tumor Microenvironment and Enhances the Efficacy of PD-L1 Checkpoint Blockade. Cell Rep 2018;22:2978–94 [PubMed: 29539425]

22. Zhang J, Bu X, Wang H, Zhu Y, Geng Y, Nihira NT, et al. Cyclin D-CDK4 kinase destabilizes PD-L1 via cullin 3-SPOP to control cancer immune surveillance. Nature 2018;553:91–5 [PubMed: 29160310]

23. Hasgur S, Aryee KE, Shultz LD, Greiner DL, Brehm MA. Generation of Immunodeficient Mice Bearing Human Immune Systems by the Engraftment of Hematopoietic Stem Cells. Methods Mol Biol 2016;1438:67–78 [PubMed: 27150084]

24. Taggart D, Andreou T, Scott KJ, Williams J, Rippaus N, Brownlie RJ, et al. Anti-PD-1/anti-CTLA-4 efficacy in melanoma brain metastases depends on extracranial disease and augmentation of CD8(+) T cell trafficking. Proc Natl Acad Sci U S A 2018;115:E1540–E9 [PubMed: 29386395]

25. Song E, Mao T, Dong H, Boisserand LSB, Antila S, Bosenberg M, et al. VEGF-C-driven lymphatic drainage enables immunosurveillance of brain tumours. Nature 2020;577:689–94 [PubMed: 31942068]

26. Nayyar N, Singh M, Stocking J, Brehm M, Brastianos P. TMOD-05. EXTRACRANIAL TUMORS INFLUENCE INTRACRANIAL RESPONSE TO IMMUNE CHECKPOINT INHIBITORS IN PRE-CLINICAL MODELS OF MELANOMA BRAIN METASTASIS. Neuro-Oncology 2020;22:ii228–ii

27. Meeth K, Wang JX, Micevic G, Damsky W, Bosenberg MW. The YUMM lines: a series of congenic mouse melanoma cell lines with defined genetic alterations. Pigment Cell Melanoma Res 2016;29:590–7 [PubMed: 27287723]

28. Sanchez VE, Lynes JP, Walbridge S, Wang X, Edwards NA, Nwankwo AK, et al. GL261 luciferase-expressing cells elicit an anti-tumor immune response: an evaluation of murine glioma models. Sci Rep 2020;10:11003 [PubMed: 32620877]

29. Zeitouni B, Tschuch C, Davis JM, Peille A-L, Raeva Y, Landesfeind M, et al. Abstract 1840: Whole-exome somatic mutation analysis of mouse cancer models and implications for preclinical immunomodulatory drug development. Cancer Research 2017;77:1840–

30. Yu JW, Bhattacharya S, Yanamandra N, Kilian D, Shi H, Yadavilli S, et al. Tumor-immune profiling of murine syngeneic tumor models as a framework to guide mechanistic studies and predict therapy response in distinct tumor microenvironments. PLoS One 2018;13:e0206223 [PubMed: 30388137]

31. Thomas R, Al-Khadairi G, Decock J. Immune Checkpoint Inhibitors in Triple Negative Breast Cancer Treatment: Promising Future Prospects. Front Oncol 2020;10:600573 [PubMed: 33718107]

32. Hu Y, Gao J, Wang M, Li M. Potential Prospect of CDK4/6 Inhibitors in Triple-Negative Breast Cancer. Cancer Manag Res 2021;13:5223–37 [PubMed: 34234565]

33. Schrors B, Boegel S, Albrecht C, Bukur T, Bukur V, Holtstrater C, et al. Multi-Omics Characterization of the 4T1 Murine Mammary Gland Tumor Model. Front Oncol 2020;10:1195 [PubMed: 32793490]
34. Dinarello CA. Historical insights into cytokines. Eur J Immunol 2007;37 Suppl 1:S34–45 [PubMed: 17972343]
35. Drouillard D, Craig BT, Dwinell MB. Physiology of chemokines in the cancer microenvironment. Am J Physiol Cell Physiol 2023;324:C167–C82 [PubMed: 36317799]
36. Turner MD, Nedjai B, Hurst T, Pennington DJ. Cytokines and chemokines: At the crossroads of cell signalling and inflammatory disease. Biochim Biophys Acta 2014;1843:2563–82 [PubMed: 24892271]
37. Choi YJ, Li X, Hydbring P, Sanda T, Stefano J, Christie AL, et al. The requirement for cyclin D function in tumor maintenance. Cancer Cell 2012;22:438–51 [PubMed: 23079655]
38. Nakajima Y, Chamoto K, Oura T, Honjo T. Critical role of the CD44(low)CD62L(low) CD8(+) T cell subset in restoring antitumor immunity in aged mice. Proc Natl Acad Sci U S A 2021;118
39. Rempala GA, Seweryn M. Methods for diversity and overlap analysis in T-cell receptor populations. J Math Biol 2013;67:1339–68 [PubMed: 23007599]
40. Scirocchi F, Scagnoli S, Botticelli A, Di Filippo A, Napoletano C, Zizzari IG, et al. Immune effects of CDK4/6 inhibitors in patients with HR(+)/HER2(−) metastatic breast cancer: Relief from immunosuppression is associated with clinical response. EBioMedicine 2022;79:104010 [PubMed: 35477069]
41. Brenner E, Schorg BF, Ahmetlic F, Wieder T, Hilke FJ, Simon N, et al. Cancer immune control needs senescence induction by interferon-dependent cell cycle regulator pathways in tumours. Nat Commun 2020;11:1335 [PubMed: 32165639]
42. Watt AC, Cejas P, DeCristo MJ, Metzger-Filho O, Lam EYN, Qiu X, et al. CDK4/6 inhibition reprograms the breast cancer enhancer landscape by stimulating AP-1 transcriptional activity. Nat Cancer 2021;2:34–48 [PubMed: 33997789]
43. Pujol JL, Vansteenkiste J, Paz-Ares Rodriguez L, Gregorc V, Mazieres J, Awad M, et al. Abemaciclib in Combination With Pembrolizumab for Stage IV KRAS-Mutant or Squamous NSCLC: A Phase 1b Study. JTO Clin Res Rep 2021;2:100234 [PubMed: 34746886]
44. Rugo HS, Kabos P, Beck JT, Jerusalem G, Wildiers H, Sevillano E, et al. Abemaciclib in combination with pembrolizumab for HR+, HER2− metastatic breast cancer: Phase 1b study. NPJ Breast Cancer 2022;8:118 [PubMed: 36335120]
45. Yuan Y, Lee JS, Yost SE, Frankel PH, Ruel C, Egelston CA, et al. Phase I/II trial of palbociclib, pembrolizumab and letrozole in patients with hormone receptor-positive metastatic breast cancer. Eur J Cancer 2021;154:11–20 [PubMed: 34217908]
46. Gong X, Litchfield LM, Webster Y, Chio LC, Wong SS, Stewart TR, et al. Genomic Aberrations that Activate D-type Cyclins Are Associated with Enhanced Sensitivity to the CDK4 and CDK6 Inhibitor Abemaciclib. Cancer Cell 2017;32:761–76 e6 [PubMed: 29232554]
47. Romero-Pozuelo J, Figlia G, Kaya O, Martin-Villalba A, Teleman AA. Cdk4 and Cdk6 Couple the Cell-Cycle Machinery to Cell Growth via mTORC1. Cell Rep 2020;31:107504 [PubMed: 32294430]
48. Scheiblecker L, Kollmann K, Sexl V. CDK4/6 and MAPK-Crosstalk as Opportunity for Cancer Treatment. Pharmaceuticals (Basel) 2020;13
49. Alhejaily A, Day AG, Feilotter HE, Baetz T, Lebrun DP. Inactivation of the CDKN2A tumor-suppressor gene by deletion or methylation is common at diagnosis in follicular lymphoma and associated with poor clinical outcome. Clin Cancer Res 2014;20:1676–86 [PubMed: 24449825]
50. Goel S, DeCristo MJ, McAllister SS, Zhao JJ. CDK4/6 Inhibition in Cancer: Beyond Cell Cycle Arrest. Trends Cell Biol 2018;28:911–25 [PubMed: 30061045]

STATEMENT OF TRANSLATIONAL RELEVANCE

Safe and effective therapies for patients with central nervous system metastases are critically needed. We show that combination CDK4/6 and PD-1 inhibition can reduce tumor burden and extend survival in immunocompetent mouse models of brain metastasis by increasing tumor immunogenicity, recruiting $CD8^+$ effector T cell subsets, depleting $CD4^+$ regulatory T cells and reducing immunosuppressive signals and T cell dysfunction. Our findings suggest that combining CDK4/6 and PD-1 inhibition is a promising therapeutic approach for enhancing immune control of intracranial metastases.

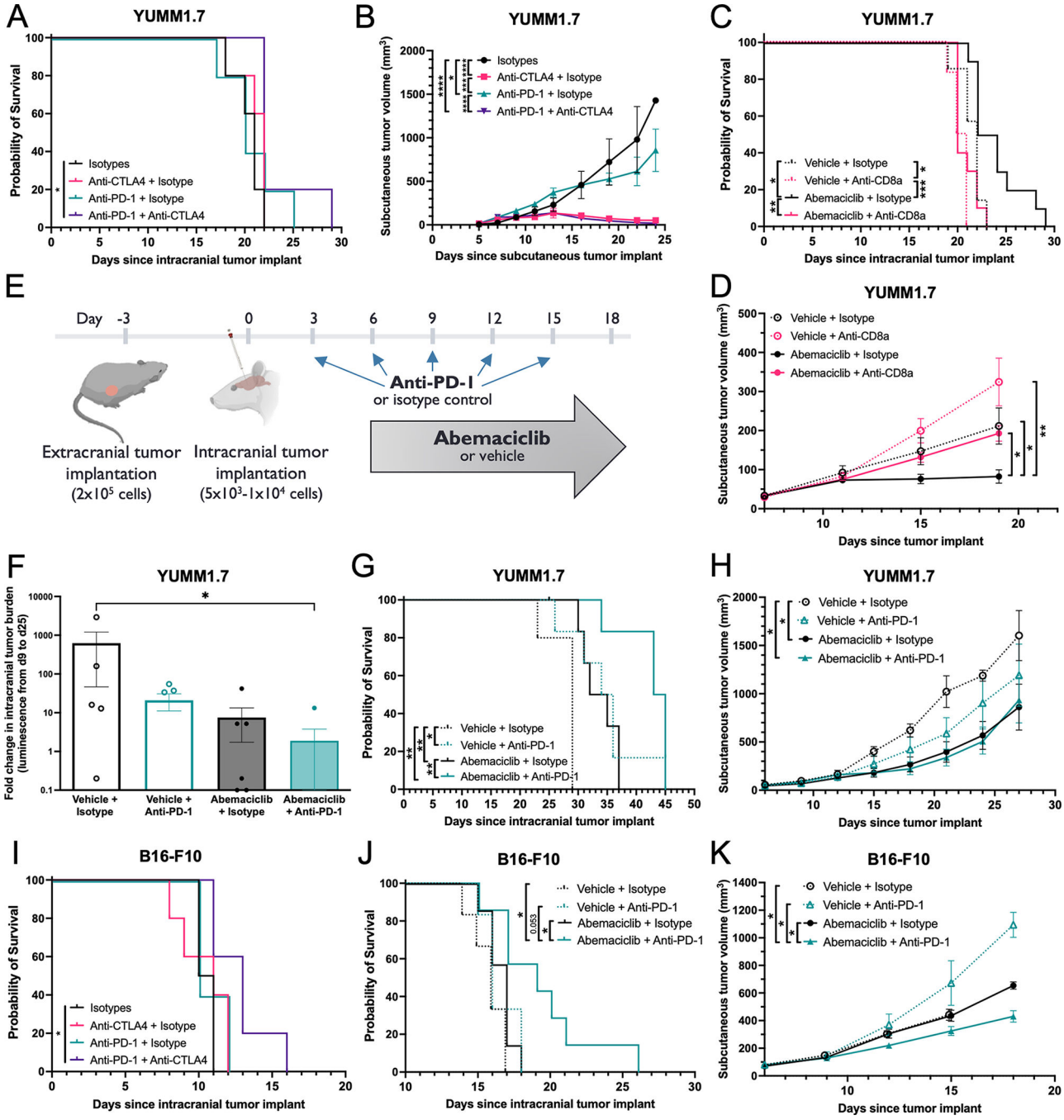

Figure 1: Combination abemaciclib and anti-PD-1 therapy reduces tumor growth and extends survival in preclinical models of CDK-mutant melanoma brain metastasis

A, Kaplan-Meier survival curve of mice bearing intracranial and subcutaneous YUMM1.7 tumors treated with single-agent or dual-agent anti-CTLA-4 and anti-PD-1 inhibition (n=5; log-rank test). **B**, Volumes of subcutaneous YUMM1.7 tumors in mice from **A** (n=5; mean ± SEM; two-way ANOVA). **C**, Kaplan-Meier survival curve of YUMM1.7 tumor-bearing mice treated with vehicle and CD8a depletion (pink dotted) or isotype control antibody (black dotted) or with abemaciclib and CD8a depletion (pink solid) or isotype control

antibody (black solid) (n=6–10; log-rank test). **D**, Volumes of subcutaneous YUMM1.7 tumors in mice from **C** (n=6–10; mean ± SEM; two-way ANOVA). **E**, Schematic of tumor implantation and treatment schedule for melanoma brain metastasis models. **F**, Change in luminescence signal of intracranial YUMM1.7 tumors 25 days after implantation (relative to day 9) in mice treated with abemaciclib and anti-PD-1 antibody as single agents or in combination (n=5–7; mean ± SEM; Kruskal-Wallis test). **G**, Kaplan-Meier survival curve of YUMM1.7 tumor bearing mice from **F**. (n=5–7; log-rank test). **H**, Volumes of subcutaneous YUMM1.7 tumors in mice from **F** and **G** (n=5–7; mean ± SEM; two-way ANOVA). **I**, Kaplan-Meier survival curve of mice bearing intracranial and subcutaneous B16-F10 tumors treated with single-agent or dual-agent anti-CTLA-4 and anti-PD-1 inhibition (n=5; log-rank test). **J**, Kaplan-Meier survival curve of mice bearing intracranial and subcutaneous B16-F10 tumors treated as above (n=6–7; log-rank test). **K**, Subcutaneous tumor volumes in mice from **J** (n=6–7; mean ± SEM; two-way ANOVA). *, $p < 0.05$; **, $p < 0.01$; ***, $p < 0.001$; ****, $p < 0.0001$.

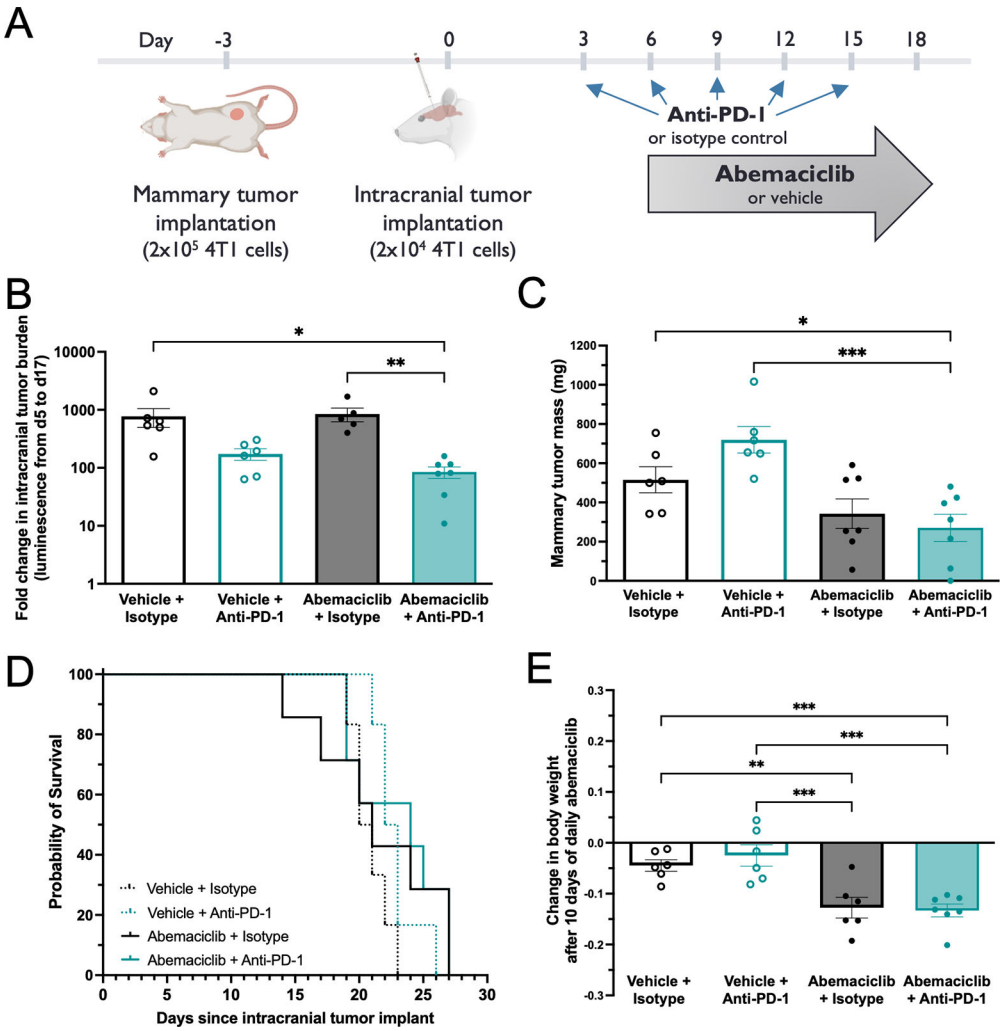

Figure 2: Combination abemaciclib and anti-PD-1 therapy reduces tumor growth in a breast cancer brain metastasis model

A, Schematic representing tumor implantation and treatment schedule for breast cancer brain metastasis model. **B**, Change in luminescence signal from intracranial 4T1 tumors treated with abemaciclib alone, anti-PD-1 alone, or combination between 5 days and 17 days after implantation (n=6–7; mean ± SEM; Kruskal-Wallis test). **C**, Mass of mammary 4T1 tumors measured at survival end point (n=6-*7;* mean ± SEM; one-way ANOVA). **D**, Kaplan-Meier survival curve of mice bearing intracranial and mammary 4T1 tumors from **B** and **C** (n=6–7; log-rank test). **E**, Change in body weight of mice from **B-D** after 10 days of daily abemaciclib dosed at 90 mg/kg (n=6–7; mean ± SEM; one-way ANOVA). *, $p < 0.05$; **, $p < 0.01$; ***, $p < 0.001$.

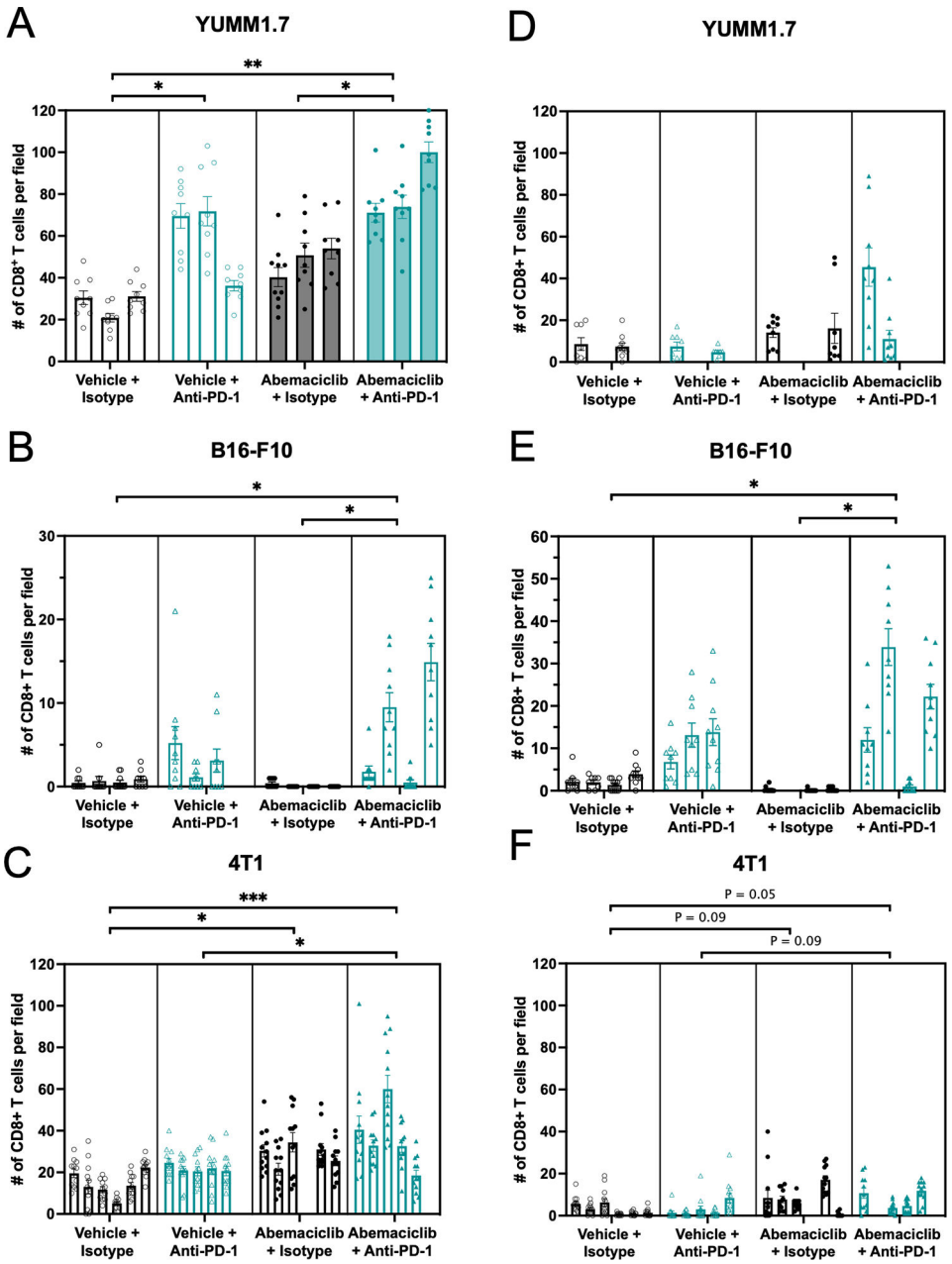

Figure 3: Combination abemaciclib and anti-PD-1 therapy drives anti-tumor inflammation into ICI resistant intracranial tumors

A-C, $CD8^+$ T cell densities in intracranial YUMM1.7 (**A**), B16-F10 (**B**) and 4T1 (**C**) tumors harvested at survival endpoint (n=3–6; mean ± SEM of number of CD8+ T cells in individual high-powered fields per tumor; nested one-way ANOVA). **D-F**, $CD8^+$ T cell densities in subcutaneous YUMM1.7 (**D**) and B16-F10 tumors (**E**) or mammary 4T1 tumors (**F**) harvested at survival endpoint (n=2–6; mean ± SEM of number of CD8+ T cells in individual high-powered fields per tumor; nested one-way ANOVA).*, $p < 0.05$; **, $p < 0.01$; ***, $p < 0.001$.

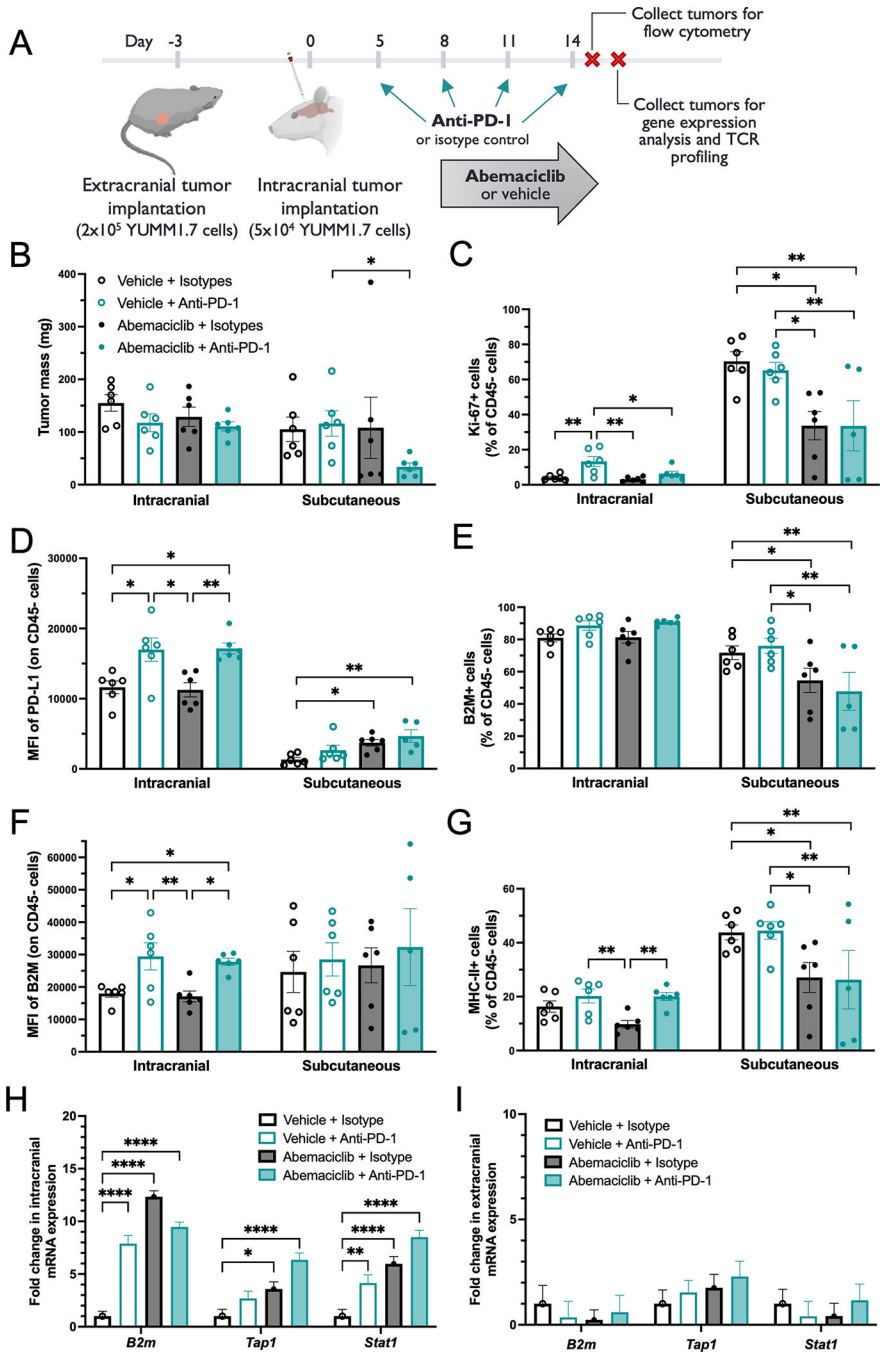

Figure 4: Combination abemaciclib and anti-PD-1 increases immunogenicity of intracranial tumors

A, Schematic showing schedule of YUMM1.7 tumor implantation, treatment and collection for flow cytometry. **B**, Mass of intracranial and subcutaneous YUMM1.7 tumors treated as indicated and harvested for flow cytometry on d15 (n=5–6; mean ± SEM; one-way ANOVA). **C**, Proportion of CD45− cells expressing Ki-67 in intracranial and subcutaneous YUMM1.7 tumors treated as indicated in **A** (n=5–6; mean ± SEM; one-way ANOVA). **D-G**, MFI of PD-L1 on CD45− cells (**D**), proportion of CD45− cells positive for B2M (**E**),

and MFI of B2M (**F**) and MHC class II (**G**) staining on CD45− cells from intracranial and subcutaneous YUMM1.7 tumors treated as indicated in **A** (n=5–6; mean ± SEM; one-way ANOVA). **H-I**, Expression of antigen presentation and interferon responsive genes in intracranial (**H**) and subcutaneous (**I**) YUMM1.7 tumors treated as described relative to vehicle treated controls (n=6; mean ± SEM; two-way ANOVA). TCR, T cell receptor; MFI, mean fluorescence intensity. *, $p < 0.05$; **, $p < 0.01$; ***, $p < 0.001$; ****, $p < 0.0001$.

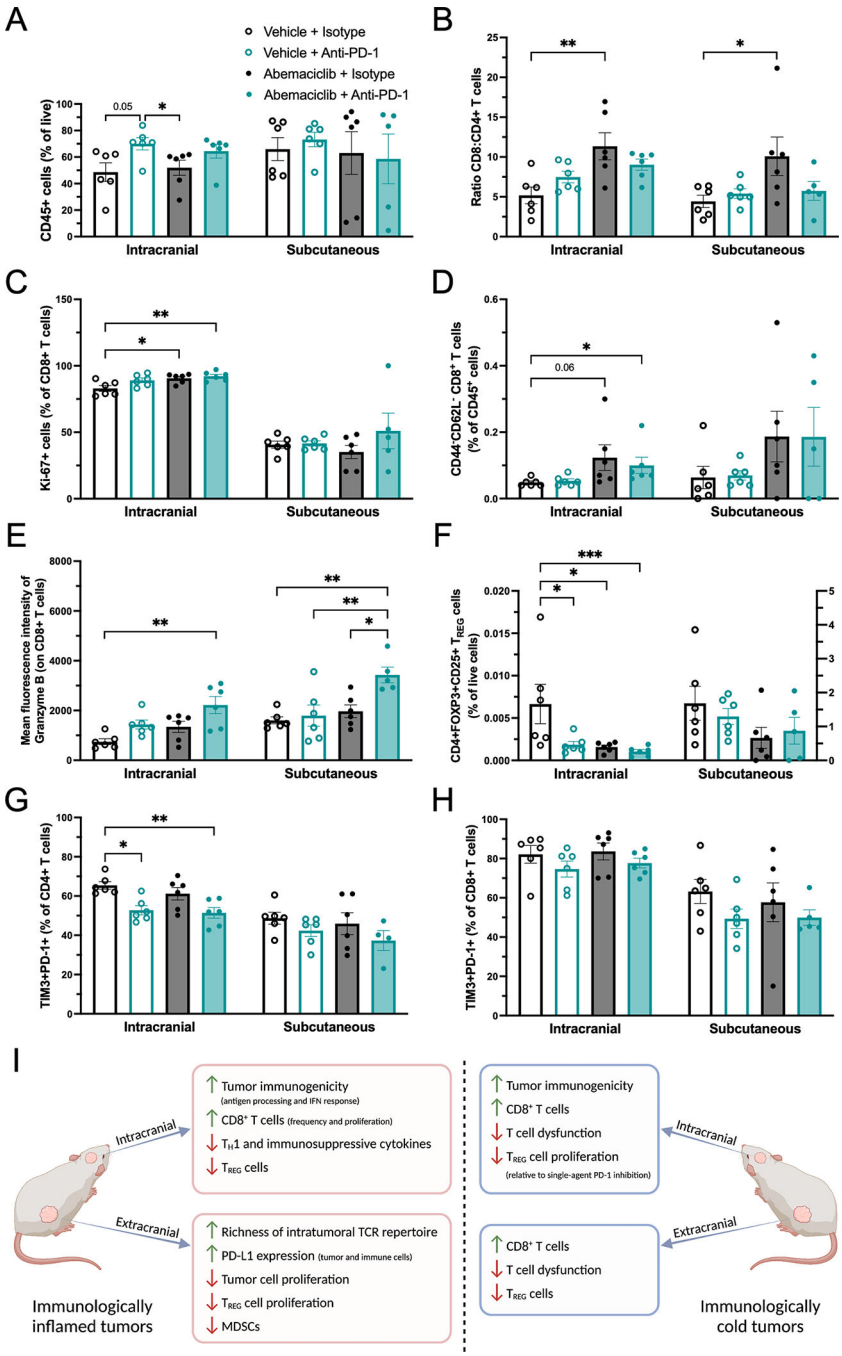

Figure 5: Combination abemaciclib and anti-PD-1 remodels the tumor immune microenvironment

A, Proportion of live cells expressing CD45 detected in intracranial and subcutaneous YUMM1.7 tumors treated as indicated (n=5–6; mean ± SEM; Kruskal-Wallis test). **B-E**, Ratio of CD8+ to CD4+ T cells (**B**), proportion of CD8+ T cells expressing Ki-67 (**C**), pre-effector-like T cell proportion of all live cells (**D**), mean fluorescence intensity of granzyme B on $CD8^+$ T cells (**E**) in intracranial and subcutaneous YUMM1.7 tumors treated as indicated in **A** (n=5–6; mean ± SEM; one-way ANOVA or Kruskal-Wallis test). **F-H**,

Regulatory T cell (T_{REG}) proportion of live cells (**F**) and TIM-3 and PD-1 co-expressing proportion of CD4+ (**G**) and CD8+ T cells (**H**) in intracranial and subcutaneous YUMM1.7 tumors treated as indicated in **A** (n=5–6; mean ± SEM; one-way ANOVA or Kruskal-Wallis test). **I**, Graphical summary showing the observed effects of combined CDK4/6 and PD-1 inhibition on tumor and immune cells that are associated with treatment efficacy in the immunogenically inflamed YUMM1.7 or immunologically cold B16-F10 dual extracranial/intracranial tumor models. ↑, increased; ↓, reduced; IFN, interferon; T_H1, T helper 1 cells; TCR, T cell receptor; T_{REG}, regulatory T cells; MDSCs, myeloid-derived suppressor cells; *, $p < 0.05$; **, $p < 0.01$; ***, $p < 0.001$.

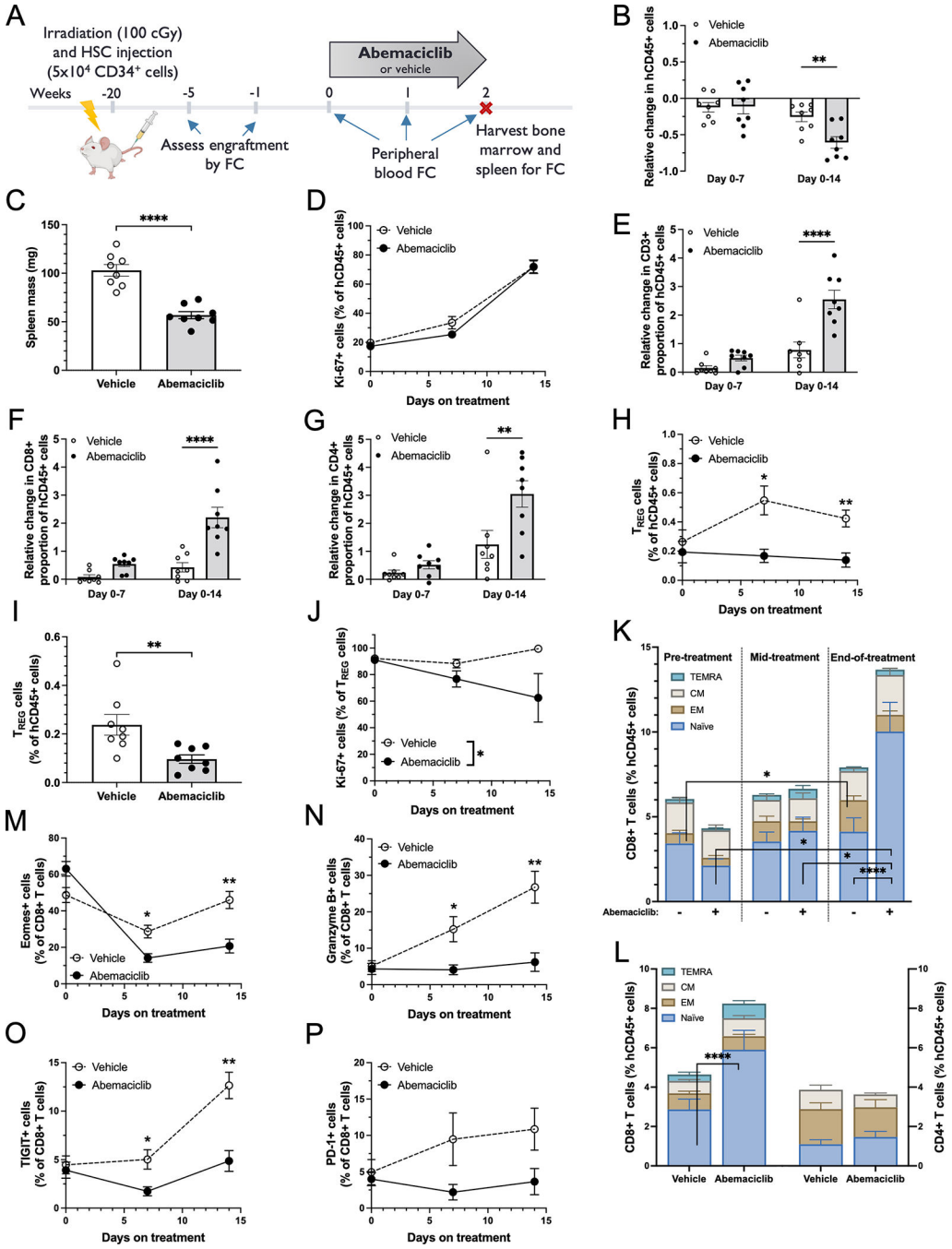

Figure 6: Abemaciclib treatment supports T cell maintenance in mice with humanized immune systems

A, Schematic showing generation of humanized mice and schedule of treatment and sample collection for flow cytometry. **B**, Relative change in frequency of hCD45+ cells detected in peripheral blood following treatment with vehicle or abemaciclib (n=8; mean ± SEM; two-way ANOVA). **C**, Mass of spleens collected from mice after 2 weeks of treatment with vehicle or abemaciclib (n=8; mean ± SEM; Student's two-tailed *t* test). **D**, Proportion of hCD45+ cells expressing Ki-67 in peripheral blood of mice treated with vehicle or

abemaciclib (n=8; mean ± SEM; two-way ANOVA). **E-G**, Relative change in CD3+ (**E**), CD8+ (**F**) and CD4+ (**G**) T cell proportion of hCD45+ cells in peripheral blood of mice treated with vehicle or abemaciclib (n=8; mean ± SEM; two-way ANOVA). H-I, T_{REG} cell proportion of hCD45+ cells in peripheral blood (**H**) or spleens (**I**) of mice treated with vehicle or abemaciclib (n=8; mean ± SEM; two-way ANOVA (**H**) or Student's two-tailed *t* test (**I**)). **J**, Proportion of T_{REG} cells expressing Ki-67 in peripheral blood following treatment with vehicle or abemaciclib (n=8; mean ± SEM; two-way ANOVA). **K**, $CD8^+$ T cell subsets as a proportion of hCD45+ cells in peripheral blood following treatment with vehicle or abemaciclib (n=8; mean ± SEM; two-way ANOVA). **L**, CD8+ (left axis) and CD4+ (right axis) T cell subsets as a proportion of hCD45+ cells in spleens collected after 2 weeks of treatment with vehicle or abemaciclib (n=8; mean ± SEM; two-way ANOVA). **M-P**, Proportion of CD8+ T cells in peripheral blood expressing EOMES (**M**), Granzyme B (**N**), TIGIT (**O**) or PD-1 (**P**) after treatment with vehicle or abemaciclib (n=8; mean ± SEM; two-way ANOVA). HSC, hematopoietic stem cell; FC, flow cytometry; hCD45+, human CD45+; T_{REG}, regulatory T; EM, effector/memory; CM, central memory; EMRA, effector/memory re-expressing CD45RA; *, $p < 0.05$; **, $p < 0.01$; ***, $p < 0.001$; ****, $p < 0.0001$.